Power Control Assessment in Induction Heating Systems with Voltage Source Inverter and Resonant L-LC Load

Mihaela Popescu, Alexandru Bitoleanu, and Alexandra Pătrașcu

Faculty of Electrical Engineering
University of Craiova
Craiova, Romania
mpopescu@em.ucv.ro, alex.bitoleanu@em.ucv.ro, apatrascu@em.ucv.ro

Abstract—The attention in this paper is directed to the power control in an induction heating system for seamless pipes consisting of a single-phase voltage source inverter with L-LC resonant load supplied by a three-phase full controlled bridge rectifier. The maximal power transfer from the inverter output to the work piece is ensured by the proper design of the matching inductor. The power control is achieved through the inverter output current by making use of a Proportional-Integrator-Derivative controller designed according to the Modulus Optimum criterion in Kessler variant. An experimental platform based on dSPACE DS1103 control board is used for the practical implementation of the control system. It works together with Matlab/Simulink environment and the conceived graphical user interface allows interacting with the experiment. The experimental setup of the induction heating system is presented and the assessment of the control system performance under different tests is performed. Depending on the prescribed value of the inverter output current and the imposed operating frequency, different situations may occur. The possibilities of diminishing the switching losses through zero-current switching and of increasing the power when the operating frequency is over the resonance value are also pointed out. All the results illustrate the proper operation and good performance of the control system.

I. INTRODUCTION

Clearly, the most common power generator adopted in the industrial applications of the energy-efficient process of induction heating (IH) is the indirect ac–ac static converter with either full-bridge current source inverter (CSI) or full-bridge voltage source inverter (VSI) [1]-[12].

Due to the advantages of VSIs, such as better converter utilization, simple limiting the switching overvoltage and simplest achievement of zero-current switching, they are preferred in the modern induction heating systems [1], [4]-[7], [11], [12], [14].

Compared to the traditional resonant load of VSI consisting of the series circuit of heating coil and compensation capacitor, the newer topology called series-parallel L-LC load leads to a smaller current through the transformer secondary and an increased short-circuit immunity [4], [5], [7], [9], [12], [13]. In this structure, a matching inductor is added at the VSI output, in series with the parallel resonant tank (the heating coil in parallel with the compensation capacitor). Thus, by adopting the parallel resonance, the current at the inverter output is an active current and the current through the induction coil is almost sinusoidal.

Referring to the operating frequency of the voltage source inverter, it is related to the resonance frequency of the resonant load and must be continuously adapted to the load conditions. Mostly, phase-locked loop (PLL) integrated circuit devices are used to track the resonant frequency throughout the system operation [12], [15].

As regards the control of the power transferred to the load, there are two possibilities. The former involves the use of a full-controlled line-commutated rectifier [4], [15], [16], whereas the latter requires charging the resonant inverter to ensure the power control in addition to the appropriate operating frequency [6], [11], [12], [17]-[19].

The induction heating system taken into consideration in this paper consists of a resonant L-LC load fed by a single-phase full-bridge VSI via a three-phase full-controlled bridge rectifier (Fig. 1).

The paper is organized as follows. Section II summarizes the adopted configuration of the induction heating system. The next section is intended to synthesize the power control circuit by making use of a transfer functions-based approach. In Section IV, the experimental setup and results of some tests are presented to validate the adopted technical solution. Finally, the main conclusions of the research are given.

II. THE SYSTEM OF INDUCTION HEATING

In this paper, the heating process of the seamless pipes is taken into consideration. The heated piece moves through the inductor at a preset speed and the required output power depends on the gradient of temperature.

As shown in Fig. 1, the parallel resonant load consists of the equivalent circuit of the induction coil and heated piece (inductance L_b and resistance R_b) in parallel with the compensation capacitor C. By means of the matching inductor (inductance L_a and resistance R_a), the power transfer from the inverter output to the induction coil is maximized [19]. The IGBTs-based single-phase full-bridge VSI provides a square wave voltage to the load circuit and the switching frequency must tracks the resonant frequency.
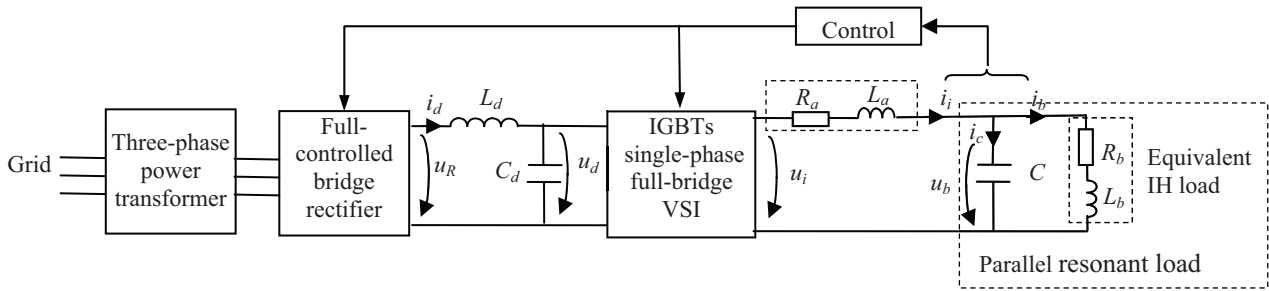
Fig. 1. Block diagram of the adopted induction heating system.

As the resonant frequency depends, on the one hand, on the heated pipe, the adopted inductor and compensation capacitance, and, on the other hand, on the dynamic variation of their parameters, an auto-adaptive frequency control loop is required. In addition, to facilitate the switching process of inverter's IGBTs through zero-current switching, the prescribed frequency should slightly exceed the resonance value.

In the adopted structure of the control system, the inverter output current is regulated through a three-phase full-controlled rectifier, in order to handle the power transmitted to the load.

III. SYNTHESIS OF THE POWER CONTROL SYSTEM

The control loop of the inverter output current is synthesized starting from the block diagram in Fig. 2. The following transfer functions are illustrated:
$G_C(s)$ - transfer function of the current controller;
$G_R(s)$ - transfer function of the three-phase full-bridge controlled rectifier;
$G_{DC}(s)$ - transfer function of the DC-link circuit;
$G_{VSI}(s)$ - transfer function of the single-phase bridge VSI;
$G_{OUT}(s)$ - transfer function of the equivalent output load;
K_{Ti} - transfer function of the current transducer.

A. The transfer Functions in the Forward Path

The three-phase full-controlled rectifier is considered as a first order element and the associated transfer function is [20]:

$$G_R(s) = \frac{U_R(s)}{U_c(s)} \approx \frac{K_R}{1 + sT_\mu}, \qquad (1)$$

where the proportional time constant (K_R) depends on the rms line-to-line voltage in the transformer secondary (U_s), i.e.
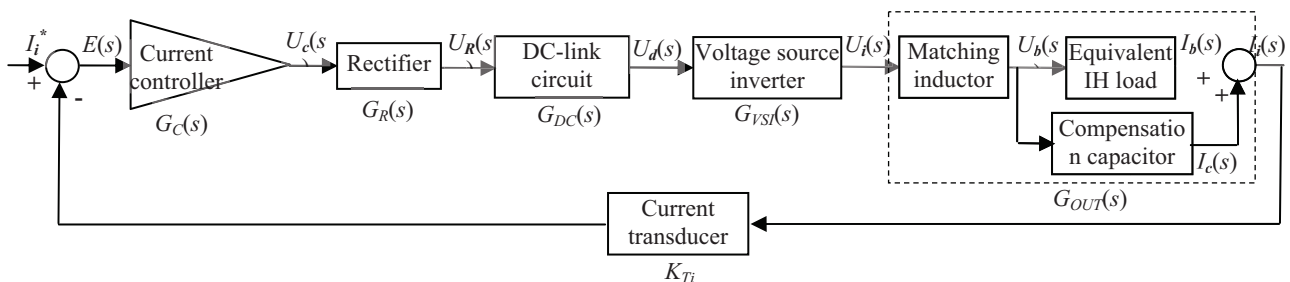
$$K_R = 3\sqrt{2} \cdot U_s / \pi, \qquad (2)$$

and the integral time constant (T_μ) is given by the average dead-time of the firing circuit and depends of the supply frequency.

The transfer function of the DC-link circuit is expressed starting from the following differential equation at the rectifier output under no load condition:

$$u_R = L_d \frac{di_d}{dt} + R_d i_d + u_d, \qquad (3)$$

where the occurring quantities are illustrated in Fig.1, except R_d, which is the DC-link resistance.

Taking into account that

$$u_d = \frac{1}{C_d} \int i_d dt, \qquad (4)$$

the Laplace transform of (3) leads to:

$$U_R(s) = L_d C_d s^2 \cdot U_d(s) + R_d C_d s \cdot U_d(s) + U_d(s). \qquad (5)$$

Thus,

$$G_{DC}(s) = U_d(s)/U_R(s) = 1/\left(1 + R_d C_d \cdot s + L_d C_d \cdot s^2\right). \qquad (6)$$

After introducing the electric (T_{ed}) and electromagnetic (T_{emd}) time constants of the DC-link circuit, i.e.

$$T_{ed} = R_d C_d. \quad T_{emd} = L_d / R_d, \qquad (7)$$

expression (6) becomes:

$$G_{DC}(s) = \frac{1}{1 + T_{ed} \cdot s + T_{emd} T_{ed} \cdot s^2}. \qquad (8)$$

The transfer function of the single-phase square wave (π radians) voltage source inverter is expressed based on the rms fundamental component of the output voltage [21],

Fig. 2. Transfer functions-based block diagram of the induction heating system.

$$U_i = \frac{2\sqrt{2}}{\pi} U_d. \qquad (9)$$

It results that G_{VSI} contains only the proportional component K_{VSI},

$$G_{VSI}(s) = K_{VSI} = \frac{U_i(s)}{U_d(s)} = \frac{2\sqrt{2}}{\pi}. \qquad (10)$$

In order to express the transfer function of the equivalent output circuit (matching inductor and resonant circuit), in terms of ratio of Laplace transforms of inverter output current and inverter output voltage, the Kirchhoff's laws in the Laplace domain are applied. Thus, the following equations are obtained:

$$U_i(s) = U_b(s) + R_a \cdot I_i(s) + s \cdot L_a \cdot I_i(s); \qquad (11)$$

$$I_i(s) = I_b(s) + I_c(s); \qquad (12)$$

$$U_b(s) = (R_b + s \cdot L_b) \cdot I_b(s); \qquad (13)$$

$$U_b(s) = \frac{1}{s \cdot C} I_c(s). \qquad (14)$$

They allow expressing $I_b(s)$ and $U_b(s)$ as a function of $I_i(s)$:

$$I_b(s) = \frac{1}{1 + s \cdot C(R_b + s \cdot L_b)} I_i(s); \qquad (15)$$

$$U_b(s) = \frac{R_b + s \cdot L_b}{1 + s \cdot C(R_b + s \cdot L_b)} I_i(s). \qquad (16)$$

After replacing (16) into (11), the equivalent output circuit transfer function is obtained in the following form:

$$G_{OUT}(s) = \frac{I_i(s)}{U_i(s)} = \frac{1}{\dfrac{R_b + s \cdot L_b}{1 + s \cdot C(R_b + s \cdot L_b)} + R_a + s \cdot L_a} = $$
$$= \frac{1}{\dfrac{R_b + s \cdot L_b}{1 + s \cdot R_b \cdot C + s^2 \cdot L_b \cdot C} + R_a + s \cdot L_a}. \qquad (17)$$

Assuming that

$$\left| \frac{R_b + s \cdot L_b}{1 + s \cdot R_b \cdot C + s^2 \cdot L_b \cdot C} \right| << |R_a + s \cdot L_a|, \qquad (18)$$

when the frequency exceeds the resonance value and after introducing the electromagnetic time constant of the matching inductor ($T_{ema} = L_a / R_a$), the final expression of $G_{OUT}(s)$ is obtained:

$$G_{OUT}(s) = \frac{1}{R_a \left(1 + \dfrac{L_a}{R_a} \cdot s\right)} = \frac{1}{R_a(1 + T_{ema} \cdot s)}. \qquad (19)$$

B. Design of Current Controller

The parameters of the inverter current controller are synthesized in accordance with the Modulus Optimum criterion in Kessler variant [16], [22].

First, the transfer function of the fixed part is expressed:

$$G_F(s) = G_R(s) \cdot G_{DC}(s) \cdot G_{VSI}(s) \cdot G_{OUT}(s) = $$
$$= \frac{K_R}{1 + sT_\mu} \cdot \frac{1}{1 + T_{ed} \cdot s + T_{emd} T_{ed} \cdot s^2} \cdot $$
$$\cdot \frac{2\sqrt{2}}{\pi} \cdot \frac{1}{R_a(1 + T_{ema} \cdot s)}. \qquad (20)$$

As it can be seen in (20), $G_F(s)$ contains two dominant time constants (T_{ed} and T_{emd}) that can be removed by choosing a PID-type current controller.

The transfer function of the adopted PID current controller is written as:

$$G_C(s) = \frac{1 + K_p T_i \cdot s + T_i T_d \cdot s^2}{T_i s}, \qquad (21)$$

where K_p is the proportional constant and T_i and T_d are the integral and derivative time constants, respectively.

Then, the attention is directed to both open-loop and closed-loop unity feedback transfer functions ($G_d(s)$ and $G_i(s)$):

$$G_d(s) = G_C(s) \cdot G_F(s) \cdot K_{Ti}; \qquad (22)$$

$$G_i(s) = \frac{G_d(s)}{1 + G_d(s)}. \qquad (23)$$

Based on (20) and (21), the final form of $G_d(s)$, i.e.

$$G_d(s) = \frac{(2\sqrt{2}/\pi) \cdot K_R \cdot K_{Ti} \cdot (1/R_a)}{sT_i \cdot (1 + sT_\mu) \cdot (1 + sT_{ema})} \cdot $$
$$\cdot \frac{(1 + K_p T_i s + T_i T_d s^2)}{(1 + sT_{ema}) \cdot (1 + T_{ed}s + T_{emd}T_{ed}s^2)}, \qquad (24)$$

allows removing the dominant time constants of the DC-link circuit through the following conditions:

$$T_{ed} = K_p T_i; \qquad (25)$$

$$T_{emd} = \frac{T_i T_d}{T_{ed}} = \frac{T_d}{K_p}. \qquad (26)$$

Next, taking into account (25), (26) and (24), the following form of (23) is obtained:

$$G_i(s) = \frac{1}{1 + \dfrac{\pi R_a}{2\sqrt{2} K_R K_{Ti}} \cdot sT_i \cdot (1 + sT_\mu) \cdot (1 + sT_{ema})}. \qquad (27)$$

According to Modulus Optimum criterion, it is found that only the coefficient K_2 of ω^2 in the denominator of expression of the square of $G_i(s)$ modulus contains a difference [22]:

$$K_2 = \frac{\pi R_a T_i}{2\sqrt{2} K_R K_{Ti}} \left[\frac{\pi R_a T_i}{2\sqrt{2} K_R K_{Ti}} - 2\left(T_\mu + T_{ema}\right) \right]. \quad (28)$$

Thus, condition of cancelling K_2 gives the expression of integral constant,

$$T_i = \frac{4\sqrt{2} K_R K_{Ti}}{\pi R_a} \cdot \left(T_\mu + T_{ema}\right). \quad (29)$$

Then, conditions (25) and (26) provide the following expressions for the proportional and derivative time constants:

$$K_p = \frac{\pi R_a T_{ed}}{4\sqrt{2} K_R K_{Ti} \cdot \left(T_\mu + T_{ema}\right)}; \quad (30)$$

$$T_d = \frac{\pi R_a T_{ed} T_{emd}}{4\sqrt{2} K_R K_{Ti} \cdot \left(T_\mu + T_{ema}\right)}. \quad (31)$$

The obtained expressions (from (29) to (31)) for the parameters of the PID controller show that they do not depend on the load parameters.

IV. POWER CONTROL SYSTEM PERFORMANCE ASSESSMENT

The assessment of the control system performance was carried out by using an experimental setup based on the electrical scheme shown in Fig. 3.

As shown, on the power supply side, there are the three-phase contactors (K_0, K_1 and K_2) allowing the general connection and the charging of the DC-link capacitor through the limiting resistors R_1.

The indirect ac–ac power converter consists of:
- a three-phase full-controlled bridge rectifier with thyristors (600 A, 1800 V); - a single-phase voltage source inverter with IGBTs (1200 A, 1700 V);
-. a DC-link circuit composed of a filtering coil (L_d) of 0.1 mH/500A and a filtering capacitor (C_d) of 2000μF/1100V).

At the inverter output, there is a matching coil of 25 turns, which is made of copper tube - Ø 24 mm and has four intermediate sockets of five turns each (Fig. 4). Its inner diameter is 270 mm and the length is 81 cm.

In order to maximize the active power transmitted to the load, the optimal number of 20 turns of the matching coil [19] was chosen for all experiments.

The capacitance of compensation capacitor is 64μF (U=3000 V, I=11.6 kA, f=10 kHz).

The working piece to be heated is a Carbon steel pipe ≈ 1% whose outer diameter is 168 cm, and wall thickness is 32mm.

In this concrete situation, the controller's parameters are: T_i= 0.366 s; T_d= 5.4·10^{-8} s; K_p=5.4·10^{-4}.

The control and management of the experimental model were performed on a dSPACE DS1103-based platform.

The control board is equipped with a PowerPC 750GX processor running at CPU clock of 1 GHz for fast floating-point calculation.

The conceived graphical user interface allows interacting with the experiment, including the imposition of the coefficient of forcing the capacitive component (K_c) in order to increase the switching frequency over the resonance frequency. In this manner, the IGBTs' zero-current switching can be achieved.
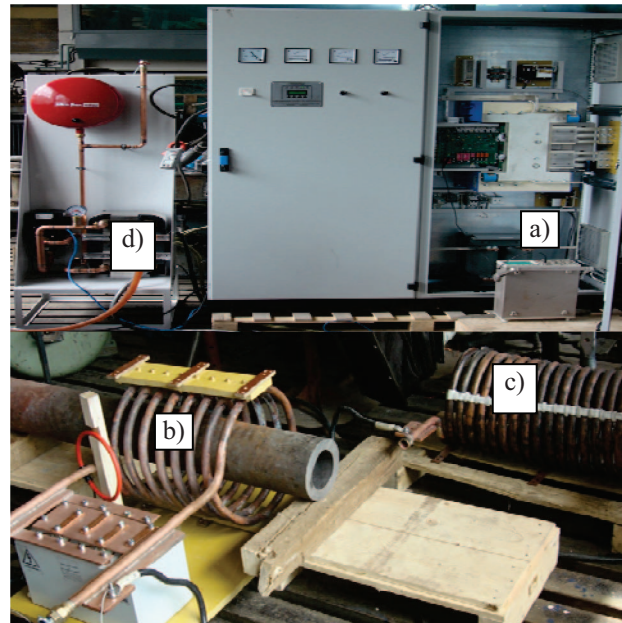

Fig. 3. Pictures of the experimental setup: a) inverter; b) inductor; c) matching coil; d) cooling equipment.
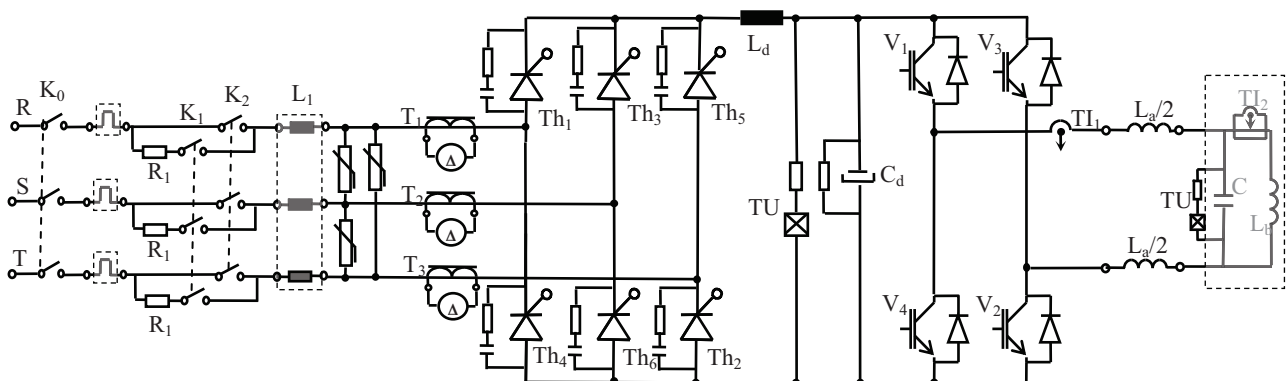

Fig. 4. The electrical scheme of the induction heating system for experimental setup.

Moreover, increasing frequency is a way of increasing the power transmitted to the load when the rectifier capability is reached.

After the system initialization process (charging the DC-link capacitor), the control system of the inverter output current is started by setting the desired value and validation of the controller output.

The control system response and the waveforms of the main quantities are provided through the graphical user interface.

In the first set of tests, the prescribed value of the inverter output current is 300 A (Fig. 5).

As shown in Fig. 5a, when the operating frequency is equal to the resonant frequency (5488 Hz), even if the maximal value the DC-link voltage (513 V) is imposed by the control loop, it is insufficient to achieve the prescribed current.

The inverter output current at resonance is low and its rms value is of about 43 A (Fig. 5a and 5b). However, by forcing the capacitive component of the current at the inverter output ($K_c = 1.38$), the prescribed current is achieved without any over-current (Fig. 5c).

The inverter input voltage fed by rectifier is maximal and the power required by the resonant load is provided by the value of the operating frequency (5918 Hz), over the resonance value.

The waveforms of voltage and current at the inverter output (Fig. 5d) indicate high switching losses, as the

zero-current switching is not achieved. It was found that the IGBTs' soft switching at zero-current corresponds to $K_c = 1.13$ (Fig. 5f), which means a switching frequency of 5651 Hz. Obviously, the set current of 300 A can not be obtained in this case (Fig. 5e).

The responses of the current controller in Fig. 6, Fig. 7 and Fig. 8 show that the minimal value of the coefficient K_c that ensures the achievement the prescribed current decreases as the prescribed current decreases. It must be noted that, in all these cases, the maximal level of the rectifier output voltage was reached.

As it can be seen in Fig. 8b compared to Fig. 6b and Fig. 7b, the set current is obtained under zero-current switching condition.

When the desired value of the inverter output current is equal to or bellow 78 A, the current control loop is able to provide the required current with minimal switching losses (zero-current switching) by a proper rectifier output voltage which is lower than 513 V. For instance, when the prescribed current is 30 A, it can be obtained at zero-current switching ($K_c =1.13$) for an inverter input voltage of 196 V (Fig. 9).

As depicted in Fig. 10, the current flowing through inductor is almost sinusoidal and in opposition to the slightly distorted current through the compensating capacitor.

As expected, the inverter output current is significantly lower than both inductor and capacitor currents.
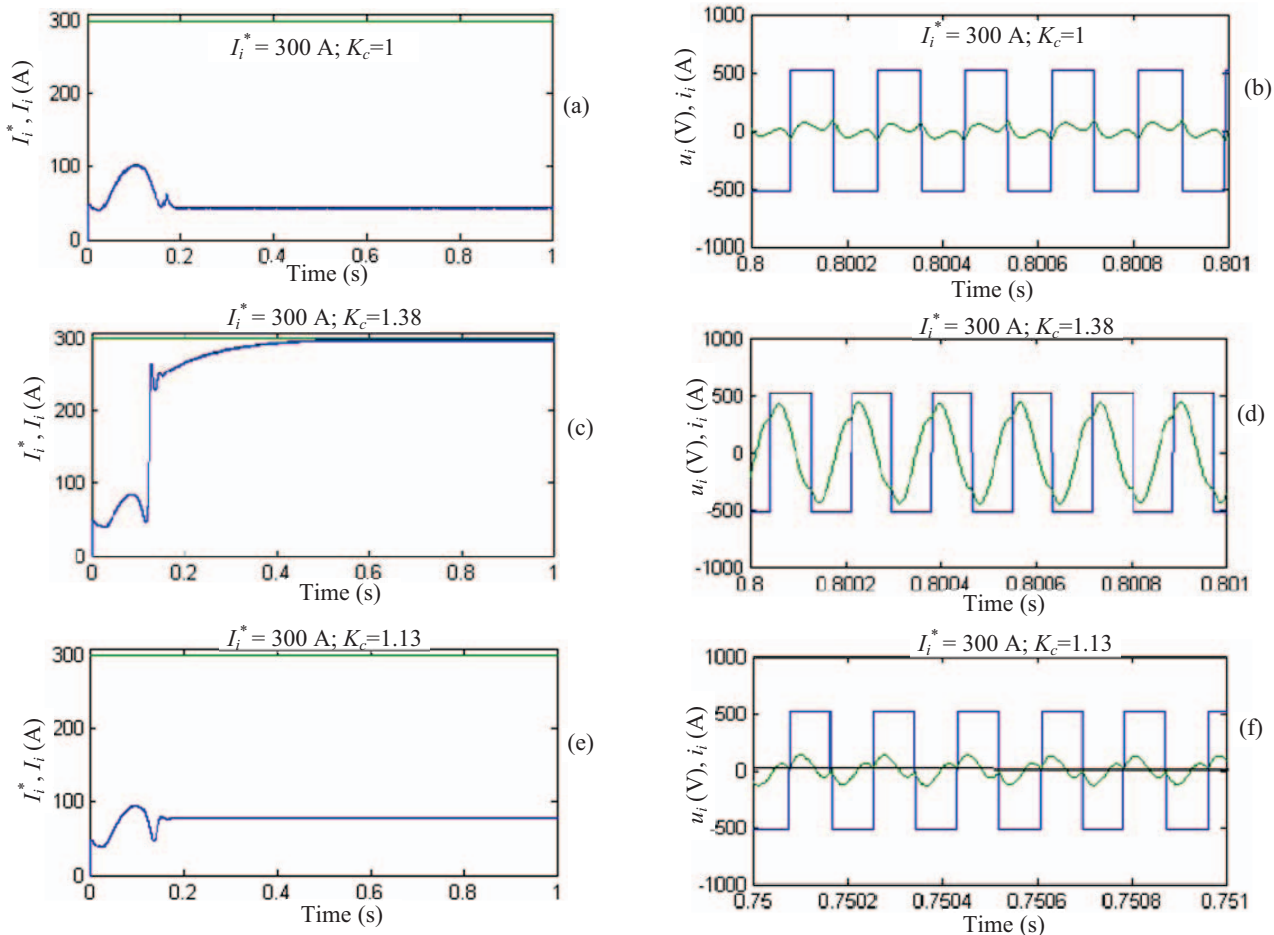

Fig. 5. Response of the current controller ((a), (c), (e)) and waveforms of voltage and current ((b), (d), (f)) at the inverter output for a prescribed current of 300A and different values of K_c.
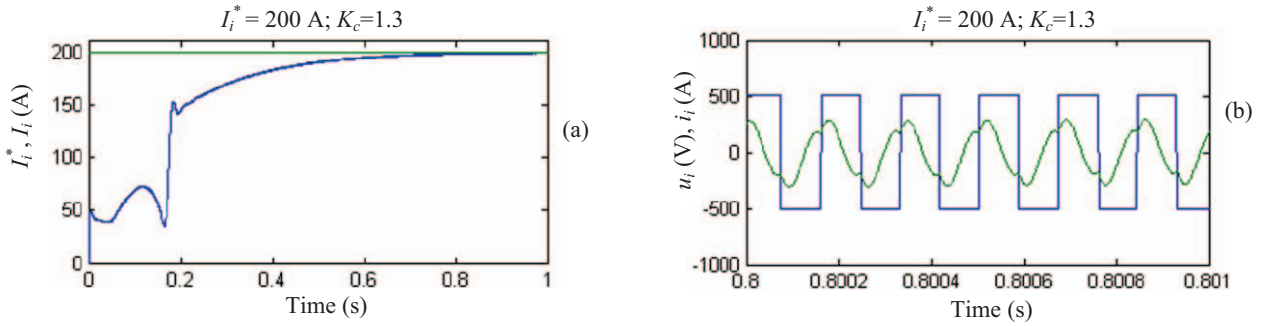
Fig. 6. Response of the current controller (a) and waveforms of voltage and current at the inverter output (b) for a prescribed current of 200A and K_c=1.3.
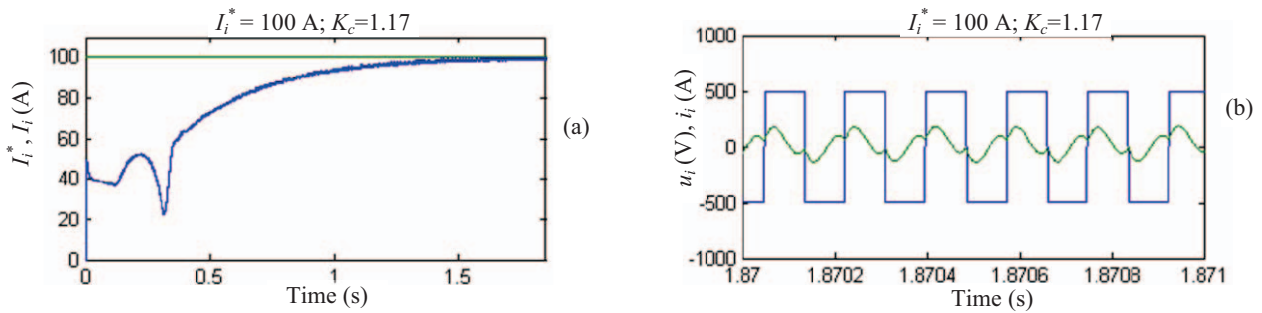

Fig. 7. Response of the current controller (a) and waveforms of voltage and current at the inverter output (b) for a prescribed current of 100A and K_c=1.17.
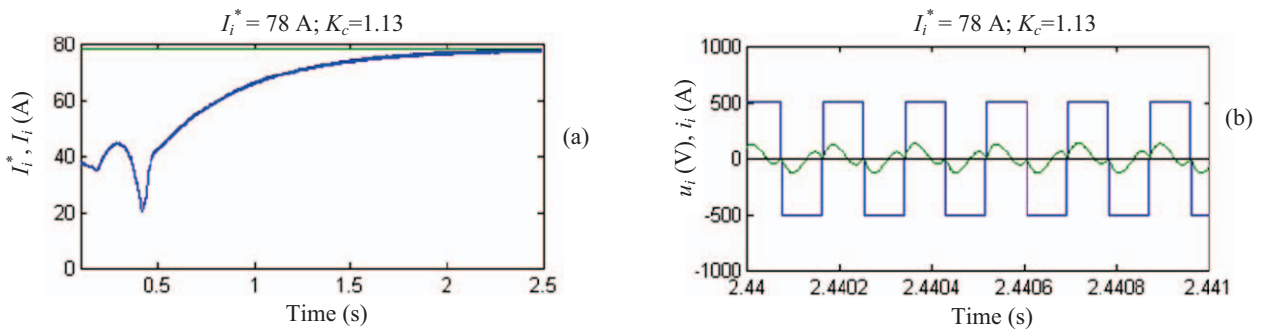

Fig. 8. Response of the current controller (a) and waveforms of voltage and current at the inverter output (b) for a prescribed current of 78A and K_c=1.13.
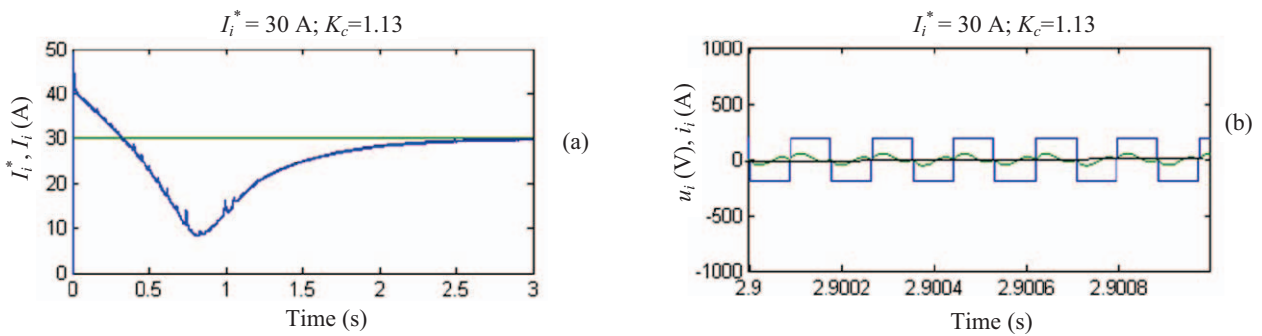

Fig. 9. Response of the current controller (a) and waveforms of voltage and current at the inverter output (b) for a prescribed current of 30A and K_c=1.13.
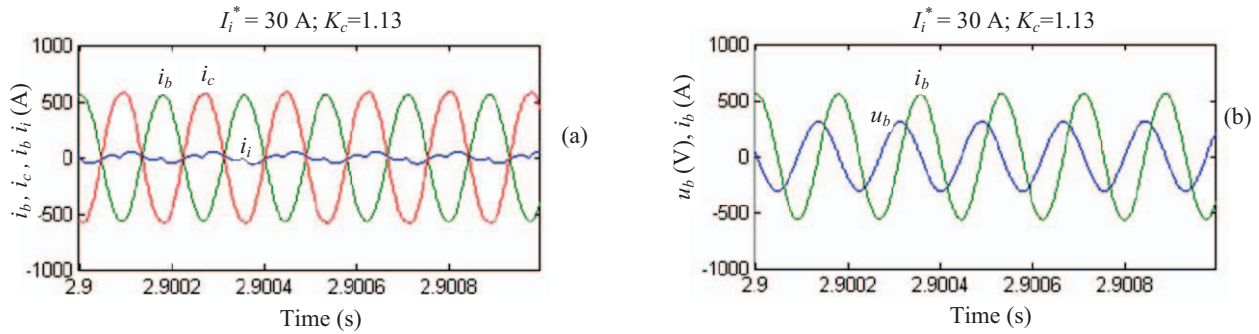
Fig. 10. Waveforms of the quantities at the inverter output for a prescribed current of 30A and K_c=1.13.

The graphical dependence in Fig. 11 illustrates the minimal values of the forcing coefficient K_c for which different prescribed currents can be obtained.

As shown, without forcing the capacitive component of the load current (K_c =1), meaning the operating at resonant frequency, a maximal current of 43 A rms can be ensured by the rectifier control.

As previously stated, by adopting K_c =1.13, the zero-current switching is obtained. In this case, the inverter can provide a maximal current of 78 A.

As the desired current increases, the required value of K_c increases and the resulted operating frequency increases.
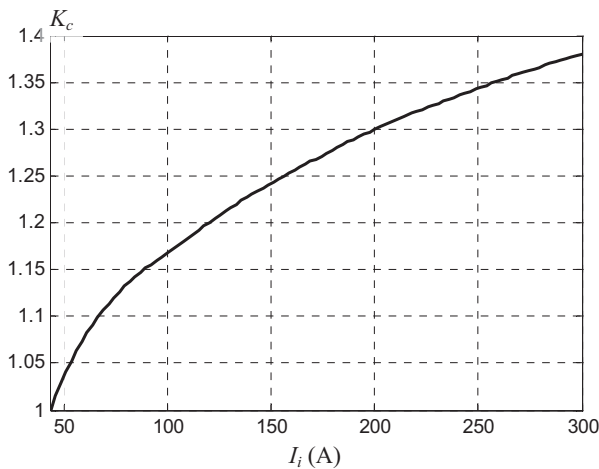

Fig. 11. Coefficient K_c versus the maximal inverter output current

V. CONCLUSIONS

In the induction heating system for seamless pipes with voltage source inverter and resonant L-LC load, the adopted control of the power transferred to the load is based on the regulation of the inverter output current.

A PID controller allowing the control of the inverter input voltage and the possibility of increasing the operating frequency over the resonant value are both taken into consideration.

It is founded that, for the resulting frequency provided by the control loop (determined by load and coefficient of forcing the capacitive component of the current), two situations may occur, i.e.:

1. The maximal DC-link voltage is insufficient to achieve the prescribed current;

2. The DC-link voltage value allows achieving the prescribed current.

For both situations, it is shown that the current control loop operates properly.

The operation at zero-current switching is obtained by increasing the control frequency over the resonance value as a result of increasing the capacitive component of the inverter current.

Starting from the finding that there are situations in which the prescribed current can not be obtained even under the maximal rectified voltage and that an increase of the inverter output current is possible by increasing the control frequency, a solution to increase the flexibility of the control system can be identified. This solution will be the subject of future investigations and can be materialized by introducing a loop for calculating the coefficient of forcing the capacitive current, based on the current error.

REFERENCES

[1] F.P. Dawson and P. Jain, "A comparison of load commutated inverter systems for induction heating and melting applications," IEEE Trans. Power Electron., vol. 6. no. 3, pp. 430-441, July 1991.

[2] A. Namadmalan, J. Shokrollahi Moghan, and J. Milimonfared, "A current-fed parallel resonant push-pull inverter with a new cascaded coil flux control for induction heating applications," Journal of Power Electronics, vol. 11, no. 5, pp. 632-638, Sept. 2011.

[3] V. Rudnev, D. Loveless, and R. Cook, Handbook of Induction Heating, Marcel Dekker, 2003, ch. 8.

[4] S. Dieckerhoff, M. J. Ryan, and R. W. De Doncker, "Design of an IGBT-based LCL resonant inverter for high-frequency induction heating, in Proc. 34th Industry Applications Conference, vol. 3, oct. 3-7, 1999, pp. 2039-2045.

[5] J.M. Espi, E.J. Dede, E. Navarro, E. Sanchis, and A. Ferreres "Features and design of the voltage-fed L-LC resonant inverter for induction heating," in Proc. Power Electronics Specialists Conference, 1999, pp. 1126 - 1131.

[6] J.M. Burdío, L.A. Barragán, F. Monterde, D. Navarro, and J. Acero, "Asymmetrical voltage-cancellation control for full-bridge series resonant inverters," IEEE Trans. Power Electron., vol. 19, no. 2, pp. 461–469, Mar. 2004.

[7] J. M. Espi Huerta, E. J. Dede Garcia Santamaria, R. Garcia Gil, and J. Castello Moreno, "Design of the L-LC resonant inverter for induction heating based on its equivalent SRI," IEEE Trans. Ind. Electron., vol. 54, no. 6, pp. 3178–3187, Dec. 2007.

[8] J. Lee, S. Lim, K. Nam, and D. Choi "An optimal selection of induction heater capacitance considering dissipation loss caused by ESR", IEEE Trans. Ind. Appl., vol. 43, no. 4, pp. 1117 – 1125, Jul./Aug. 2007.

[9] E. Zok, D.M. Schibisch, "Energy-efficient power supply for induction hardening and heating processes," in Induction Technology Reports, no. 1, 2013, pp. 67-74.

[10] A. Namadmalan and J.S. Moghani, "Tunable self-oscillating switching technique for current source induction heating systems," IEEE Trans. Ind. Electron., vol. 61, no. 5, pp.2556–2563, May 2014.

[11] V. Esteve, J. Jordán, E. Sanchis-Kilders, E.J. Dede, E. Maset, J.B. Ejea, and A. Ferreres, "Improving the reliability of series resonant inverters for induction heating applications," IEEE Trans. Ind. Electron., vol. 61, no. 5, pp. 2564–2572, May 2014.

[12] S. Chudjuarjeen, A. Sangswang, and C. Koompai, "An improved LLC resonant inverter for induction-heating applications with asymmetrical control," IEEE Trans. Ind. Electron., vol. 58, no. 7, pp. 2915–2925, Jul. 2011.

[13] J.M. Espi, E.J. Dede, A. Ferreres, and R. Garcia, "Steady-state frequency analysis of the LLC- resonant inverter for induction heating,", in Technical Proc. V IEEE Int. Power Electronics Congress, 14-17 Oct. 1996, pp. 22-28.

[14] A. Salih, "IGBT for high performance induction heating applications," in Proc. 38th Annual Conference on IEEE Industrial Electronics Society, Oct. 2012, pp. 3274-3280.

[15] A. Okuno, H. Kawano, J. Sun, M. Kurokawa, A. Kojina, and M. Nakaoka., "Feasible development of soft-switched SIT inverter with load-adaptive frequency-tracking control scheme for induction heating," IEEE Trans. Ind. Appl., vol. 34, no. 4, pp. 713–718, Jul./Aug. 1998.

[16] Mihaela Popescu and A. Bitoleanu A., "Power control system design in induction heating with resonant voltage inverter," Journal of Automation and Control Engineering, vol. 2, no. 2, pp. 195-198, June 2014.

[17] P. Viriya, S. Sittichok, and K. Matsuse, "Analysis of high-frequency induction cooker with variable frequency power control," in Proc. PCC Osaka, Apr. 2002, vol. 3, pp. 1502–1507.

[18] X. Ruan, W. Chen, L. Cheng, C.K. Tse, H. Yan, and T. Zhang, "Control strategy for input-series–output-parallel converters," IEEE Trans. Ind. Electron., vol. 56, no. 4, pp. 1174–1185, Apr. 2009.

[19] A. Bitoleanu, Mihaela Popescu, and V. Suru, "Maximizing power transfer in induction heating system with voltage source inverter," in Proc. 22nd Int. Conf. on Nonlinear Dynamics of Electronic Systems, Albena, Bulgaria, July 4-6, 2014, vol. 438, pp. 134-141.

[20] G. Sieklucki, "Analysis of the transfer-function models of electric drives with controlled voltage source," Przeglad Elektrot., no. 7a, pp. 250-255, 2012.

[21] A. Bitoleanu A., S. Ivanov, and M. Popescu, Convertoare statice, Infomed Craiova, 1997.

[22] A.J.J. Rezek, C.A.D. Coelho, J.M.E.Vicente, J.A. Cortez , and P.R. Laurentino, "The modulus optimum (MO) method applied to voltage regulation systems: modeling, tuning and implementation," in Proc. Int. Conf. on Power System Transients, June 2001, pp. 138-142.